Structure and Reactivity Studies of $CoHNO^+$ in the Gas Phase

Huiping Chen,† Denley B. Jacobson,* and Ben S. Freiser‡

H. C. Brown Laboratory of Chemistry, Purdue University, West Lafayette, Indiana 47907

Received: June 3, 1999; In Final Form: August 26, 1999

The structure and energetics of three $CoHNO^+$ isomers [$HCo(NO)^+$ (**1**), $Co(HNO)^+$ (**2**), $Co(NOH)^+$ (**3**)] were probed by using density functional theory (DFT). Theory predicts that **2** is the most stable structure with **1** and **3** 14.1 and 15.4 kcal/mol less stable. We were unable to locate the transition states for **2** → **1** and **2** → **3** conversions. DFT calculations predict $D°(CoH^+-NO) = 34.6$ kcal/mol and $D°(Co^+-HNO) = 45.5$ kcal/mol. The gas-phase ion chemistry of $CoHNO^+$ was also studied by using Fourier transform ion cyclotron resonance (FTICR) mass spectrometry. CID and SORI−CID of $CoHNO^+$ yield competitive formation of Co^+, CoH^+, and $CoNO^+$. These results suggest that the barrier for **2** → **1** conversion is less than 45.5 kcal/mol. Reactions with simple molecules were dominated by NO and HNO displacements. Potential energy surface diagrams are presented to explain these displacement reactions. Surprisingly, $CoHNO^+$ reacts with methane by dehydrogenation to yield $CoCH_3NO^+$. Studies suggest CH_3CoNO^+ rather than $Co(CH_3NO)^+$ as the structure for this ion.

Introduction

Intramolecular hydrogen transfer from a transition metal center to an unsaturated ligand, and the reverse process, hydride migration from an organic ligand back to the metal center, are ubiquitous processes in organometallic chemistry.[1] Hydride migration to an alkene or an alkyne is a key step in homogeneous hydrogenation and in many alkene and alkyne alkylation processes. Hydride migrations to simple ligands such as C_2H_4[2,3] and CH_2O[4,5] have been extensively studied, and the reverse process (i.e., β-H elimination) is often found to be facile. In contrast to β-H elimination/insertion reactions, α-H elimination/insertion reactions are not so common. For example, the hydride migration to the carbonyl ligand (i.e., CO insertion) is known only for a few cases in transition metal complexes.[6,7] One of the known examples is the formyl formation by carbonyl insertion into the Rh−H bond, reaction 1.[8]

$$Rh(OPE)(H) + CO \rightarrow Rh(OEP)(CHO) \quad (1)$$

Generally the CO insertion processes have been studied by theory because of experimental limitations. The hydride migration to a carbene type ligand and the reverse α-H elimination have also drawn the attention of many theoreticians.[9] Ziegler and co-workers studied the CH_2 insertion into a Mn−H bond, reaction 2, and found that it is much more exothermic than the corresponding hydride migrations to CO or CS.[10] Carter and Goddard studied reaction 3 by theory and predicted an activation barrier of 12 kcal/mol with an exothermicity of 7 kcal/mol for the carbene insertion into the Ru−H bond.[11]

$$HMn(CO)_4(CH_2) \rightarrow Mn(CO)_4CH_3 \quad (2)$$

$$ClRu(H)(CH_2) \rightarrow ClRu(CH_3) \quad (3)$$

Nitric oxide (NO) is the simplest, thermally stable paramagnetic molecule known. The binding of nitric oxide to a metal center imparts unique chemistry to both the metal center and the nitrosyl ligand. Despite extensive experimental and theoretical studies carried out on metal−nitrosyl complexes,[12] little is known about hydride migration to the nitrosyl ligand. Reduction of the NO ligand on the metal center by hydride migration can yield two products, M-nitrosyl hydride (M-HNO) and M-hydroxyimido (M-NOH), reaction 4. In a previous study, the coordinated HNO ligand in reaction 5 has been characterized by X-ray methods.[13] Transformation of a NO ligand to a NOH ligand has also been observed, reaction 6.[14]

$$H-M-NO \rightarrow M-HNO \rightarrow M-NOH \quad (4)$$

$$Os(NO)Cl(CO)(PPh_3)_2 + HCl \rightarrow Os(HNO)Cl_2(CO)(PPh_3)_2 \quad (5)$$

$$[Ru_3(CO)_{10}(\mu_2\text{-}NO)]^- + H^+ \rightarrow [Ru_3(CO)_{10}(\mu_3\text{-}NOH)] \quad (6)$$

Hydride migration to the NO ligand for the transition metal complexes has not been studied in the gas phase. Investigation of reaction 4 in the gas phase provides a unique opportunity for studying both β-H and α-H eliminations within an individual organometallic system without complicating effects from other ligands. Here, we study the [Co, H, N, O]$^+$ system by using Fourier transform ion cyclotron resonance (FTICR) mass spectrometry. A comprehensive theoretical investigation of different $CoHNO^+$ isomers [$HCo(NO)^+$ (**1**), $Co(HNO)^+$ (**2**), and $Co(NOH)^+$ (**3**)] was performed by using density functional theory (DFT).

$$\underset{\mathbf{1}}{H-Co^+-NO} \quad \underset{\mathbf{2}}{Co^+-HNO} \quad \underset{\mathbf{3}}{Co^+-NOH}$$

Experimental Section

All experiments were performed by using a Nicolet (now Finnigan FT/MS, Madison, WI) FTMS-2000 Fourier transform

* Corresponding author. Department of Chemistry, North Dakota State University, Fargo ND 58104.

† Present address: Wyeth-Ayerst Research, Lederle Laboratories, 401 N. Middletown Road, Bldg. 222/1044, Pearl River, NY 10965.

‡ Deceased December 31, 1997.

10.1021/jp991791y CCC: $18.00
Published on Web 11/30/1999

ion cyclotron resonance (FT-ICR) mass spectrometer equipped with a dual trapping cell with a 3-T superconducting magnet. A complete description of the instrument is given elsewhere.[15]

Chemicals were obtained commercially in high purity and were used as supplied except for multiple freeze−pump−thaw cycles to remove noncondensable gases from liquids. Methane was introduced into the vacuum chamber via a Varian leak valve at a static pressure of $\sim 1.5 \times 10^{-7}$ Torr as the reagent gas for chemical ionization. Ar was added to the cell to a total pressure of $\sim 5.0 \times 10^{-6}$ Torr and serves, with background methane, as the collision gas for collision-induced dissociation (CID)[16] and sustained off-resonance irradiation (SORI)[17] CID experiments. Ar also facilitates ion thermalization for reaction studies.

The maximum translational energy acquired during CID by the ions, $E_{tr}(max)$, is given in the laboratory frame and was calculated by using the following equation applicable to a cubic cell where E is the electric field amplitude, t is the duration of the applied electric field, q is the ion charge, and M_{ion} is the mass of the irradiated ion.[18,19]

$$E_{tr}(\max) = \frac{E^2 q^2 t^2}{16 M_{ion}}$$

CID fragment ion intensities are plotted as a fraction of the total ion intensity at each kinetic energy. The duration of the excitation pulse is 500 μs with the electric field amplitude varied to control ion kinetic energy. A 50 ms delay follows ion irradiation to allow for ion collisions and decomposition prior to subsequent isolation or detection.

In addition to conventional FTICR−CID, CID by using sustained "off-resonance" irradiation (SORI)[17] for ion activation was also employed to determine the lowest energy fragmentation pathways. For SORI−CID, ions are irradiated off-resonance for 500 ms. The *maximum* ion kinetic energy is calculated by using the following equation:

$$E_{tr}(\max) = \frac{E^2 q^2}{2 M_{ion} (\omega_1 - \omega_c)^2}$$

where ω_1 (rad s^{-1}) is the excitation frequency and ω_c is the natural cyclotron frequency of the ion.

For kinetic studies, neutral reagents were introduced into the vacuum chamber through Varian leak valves. Pressure of neutrals was measured by using a Bayard−Alpert type ion gauge that was calibrated to determine the pressure gradient between the reaction cell and ion gauge. Pressure was also corrected for ionization sensitivities. The uncertainty in the absolute pressure of neutral reagents is less than ±30%. The uncertainty in pressure is the largest contributor to errors in reaction rate constants. Consequently, we assign an absolute error of ±30% for reaction rate constants, while relative reaction rate constants are more reliable.

Computational Studies

Calculations were performed with the *Gaussian 94* DFT program package[20] at the Purdue University Computer Center (PUCC). Both the ground and excited states of the [Co, H, N, O]$^+$ system were investigated by using density functional theory. For the computational studies, a hybrid of DFT and Hartree−Fock (HF) was applied in which the Becke-3-LYP (B3LYP) functional[21] was used for the exchange correlation functional. For cobalt, the (14s9p5d) primitive set of Wachters[22] supplemented with one diffuse p-function, one diffuse d-function, and one diffuse f-function according to Bauschlicher[23] is used, resulting in a (62111111|331211|3111|3) → [8s6p4d1f] contraction. The cc-pVTZ basis set[24] was employed for H, N, and O atoms. For Co^+, B3LYP gives the correct ordering of atomic states, but because of the bias toward $3d^n$ over $4s^1 3d^{n-1}$ configurations,[25] the excitation energy to the ^5F ($4s^1 3d^7$) state is overestimated by 5.8 kcal/mol (calculated, 15.7; experimental, 9.9 kcal/mol). The DFT/HF hybrid method yields molecular geometries which are qualitatively comparable with those obtained at highly correlated levels.[26] The computed thermochemistry is reasonable; however, the bond dissociation energies (BDEs) tend to be slightly overestimated. Therefore, the accuracy of the DFT/HF approach for transition-metal compounds is estimated to be within ±10 kcal mol^{-1} for BDEs and ±5 kcal mol^{-1} for the relative energies of isomeric [Co, H, N, O]$^+$ species. All stationary points were characterized as minina or first-order transition structures by evaluating the frequencies and normal modes by using analytical first derivatives and the computed force constant matrix. Corrections for zero point energies are included, and different spin configurations have also been considered for Co^+.

Results and Discussion

Computational. Structures **1**, **2**, and **3** are considered for $CoHNO^+$ isomers. Density functional calculations were performed on each structure and all were found to be true minima on the potential energy surface. Table 1 contains the relative energies of $CoHNO^+$ isomers for the ground and low-lying excited states.

TABLE 1: Relative Energies of the Ground State and Excited States of Structures 1, 2, and 3

structure	relative energy (kcal/mol)
1 (^{3}A′)	14.1
1 (^{1}A′)	25.7
1 (^{5}A″)	35.1
2 (^{3}A′)	0
2 (^{5}A′)	13.8
2 (^{1}A′)	36.2
3 (^{3}A′)	15.4
3 (^{5}A′)	18.2
3 (^{1}A′)	35.0

1. HCo(NO)$^+$. Among the three reasonable isomers, we first consider the H−Co^+−NO structure, **1**. The optimized geometries of **1** (^{5}A″), **1** (^{3}A′), and **1** (^{1}A′) are shown in Figure 1. Structure **1** (^{3}A′) is the ground state, with **1** (^{1}A′) and **1** (^{5}A″) 11.6 and 21.0 kcal/mol higher, respectively. The Co−N bond lengths vary from 1.841 Å **1** (^{3}A′), 2.174 Å in **1** (^{5}A″), and 1.615 Å in **1** (^{1}A′). The extremely long Co−N distance in **1** (^{5}A″) suggests an ion−dipole complex. Unlike the Co−N bond, the N−O bonds vary by no more than 0.03 Å from the N−O bond length of 1.146 Å for free NO. In **1** (^{3}A′), the Co−H bond is bent toward the NO ligand with an H−Co−N bond angle of 139.0°. In **1** (^{1}A′), the Co−H bond is bent further with an H−Co−N bond angle of only 83.3°. Strengthening of the N−O bond is observed as evidenced by the calculated N−O stretches (2029 cm^{-1} in **1** (^{3}A′) and **1** (^{5}A″) compared to 1977 cm^{-1} calculated for free NO). The dissociation energy to form CoH^+ ($^4\Phi$) and NO ($^2\pi$) from H−Co^+−NO (^{3}A′) is computed to be 34.6 kcal/mol and compares well with $D°(Co^+-NO) = 40.0$ kcal/mol[27] calculated by Bauschlicher and co-workers.

As typical for metal−nitrosyl complexes, both bent and linear geometries of the Co^+−NO component are observed for the ground and excited states of $HCo(NO)^+$. Clearly, Co^+ binds NO in a bent geometry in **1** (^{3}A′) and **1** (^{5}A″), and in an almost linear fashion in the low-lying excited state, **1** (^{1}A′). With a

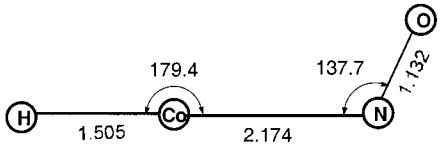

1 (^{5}A'', C_s)

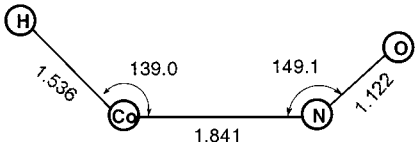

1 (^{3}A', C_s)

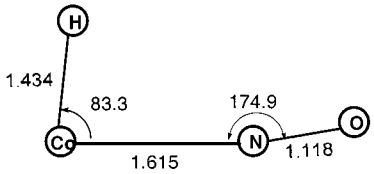

1 (^{1}A′, C_s)

Figure 1. Optimized geometries of the quintet, triplet, and singlet states of $HCo(NO)^+$ (bond lengths in Å and bond angles in degrees).

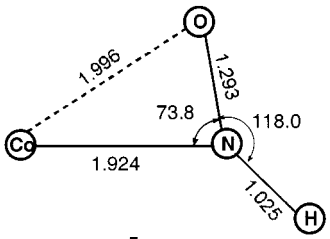

2 (^{5}A', C_s)

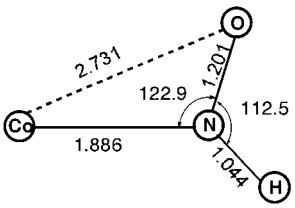

2 (^{3}A', C_s)

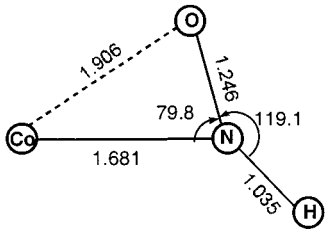

2 (^{1}A', C_s)

Figure 2. Optimized geometries of the quintet, triplet, and singlet states of $Co(HNO)^+$ (bond lengths in Å and bond angles in degrees).

bent geometry in **1** (^{3}A′) and **1** (^{5}A″), the N and O atoms are sp^2 hybridized and the coordination of NO to the metal center involves a net donation of one electron from NO to the metal. However, the almost linear geometry in **1** (^{1}A′) suggests that the coordination of NO to Co^+ involves a net donation of three electrons. In this case, strengthening of the Co^+-N bond can be seen in the shortened Co−N bond length of 1.615 Å.

2. Co(HNO)$^+$. The optimized geometries for the ground and two excited states of **2** are shown in Figure 2. Structure **2** (^{3}A′) is the global minimum on the potential energy surface of the $[Co, H, N, O]^+$ system. Structure **2** (^{3}A′) has C_s symmetry with a Co−N bond length of 1.886 Å. The N−O bond distance is 1.201 Å and the N−H bond distance is 1.044 Å. The experimental values, are, respectively, 1.212 and 1.063 Å for the free HNO molecule.[28] The HNO unit of **2** (^{3}A′) has a bent geometry with the H−N−O bond angle of 112.5°, compared to 108.7° in free HNO by calculations. The N−O bond is probably a double bond as evidenced from the longer N−O bond versus free NO (1.156 Å).[29] The dissociation energy to form Co^+ (^{3}F) and singlet HNO (^{1}A′) is predicted to be 45.5 kcal/mol with zero point energy corrections. As shown in Table 1, **2** (^{3}A′) is 14.1 kcal/mol more stable than the α-H migration product, **1** (^{3}A′). Although the transition state connecting **1** (^{3}A′) and **2** (^{3}A′) was not located, the activation barrier for the α-H migration is believed to be less than 40 kcal/mol with respect to **2** (^{3}A′), *vide infra*.

The two excited states, **2** (^{5}A′) and **2** (^{1}A′), are 13.8 and 36.2 kcal/mol less stable than **2** (^{3}A′), respectively. They both have C_s symmetry and exhibit similar structural features. A much smaller Co−N−O bond angle (73.8° in **2** (^{5}A′) and 79.8° in **2** (^{1}A′)) is observed, compared to 122.9° for the ground state. The Co^+-O distance for the two excited states is much smaller than that in the ground state. The two excited states have a side-on bonding with NO of the HNO molecules. This interaction can be described by the Dewar−Chatt−Duncanson model. Donation of π-electron density from NO along with π-back-donation from the metal into π* orbital result in weakening of the NO bond. This NO bond weakening is manifested in an increase in the NO bond lengths for the two excited states (Figure 2).

3. Co(NOH)$^+$. The triplet state (^{3}A′) is only 2.8 kcal/mol lower in energy than the quintet state (^{5}A′) of $Co(NOH)^+$. Since they are so close together, we cannot assign which is the ground state. Structure **3** (^{3}A′) and **3** (^{5}A′) both have C_1 symmetry and similar structures. The Co−N bond distance of **3** (^{3}A′) is 1.755 Å, and the N−O distance is 1.279 Å, compared to 1.810 and 1.289 Å in **3** (^{5}A′). The Co−N−O bond angle in **3** (^{3}A′) is 122.9° compared to 144.2° in **3** (^{5}A′). The singlet state, **3** (^{1}A′), is 19.6 kcal/mol less stable than the triplet state. Structure **3** (^{1}A′) has a Co−N−O bond angle of 153.2° and a much shorter Co−N bond distance of 1.561 Å. The N−O bond is also decreased to 1.266 Å.

The ground-state HNO isomer is about 24 kcal/mol more stable than the corresponding NOH isomer.[30] On the triplet surface, the $Co(NOH)^+$ structure is only 1.3 kcal/mol less stable than the $H-Co^+-NO$ structure, and is 15.4 kcal/mol less stable than the $Co(HNO)^+$ structure. Conversion of **3** (^{3}A′) to **1** (^{3}A′) involves a β-H transfer from the hydroxyimido ligand to the metal center and is essentially thermoneutral. Unfortunately, the transition structure connecting **3** (^{3}A′) and **1** (^{3}A′) was not located. However, the $CoHNO^+$ ions, once generated and thermalized in the gas phase, are most likely structure **2**,

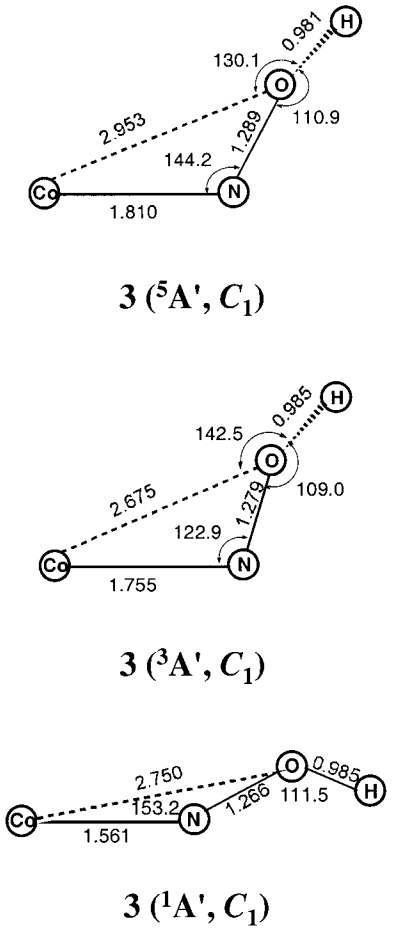

Figure 3. Optimized geometries of the quintet, triplet, and singlet states of Co(NOH)$^+$ (bond lengths in Å and bond angles in degrees).

Co(HNO)$^+$. Consequently, **3** (^{3}A′) to **1** (^{3}A′) conversion is probably unimportant.

Experimental. *1. Generation and Characterization of CoHNO*$^+$. In light of the high volatility of Co(CO)$_3$(NO) at room temperature, the synthesis of CoHNO$^+$ is relatively simple. CoHNO$^+$ can be generated from CID or sequential SORI−CID of protonated cobalt tricarbonyl nitrosyl [HCo(CO)$_3$NO$^+$], reaction 7 or 8. HCo(CO)$_3$NO$^+$ was generated by chemical ionization of Co(CO)$_3$NO with CH_5^+.

$$\mathrm{HCo(CO)_3NO^+} \xrightarrow{\mathrm{CID}} \mathrm{CoHNO^+ + 3CO} \qquad (7)$$

$$\mathrm{HCo(CO)_3NO^+} \xrightarrow[-\mathrm{CO}]{\mathrm{SORI}} \xrightarrow[-\mathrm{CO}]{\mathrm{SORI}} \xrightarrow[-\mathrm{CO}]{\mathrm{SORI}} \mathrm{CoHNO^+} \qquad (8)$$

Several precursor ions, CoH(CO)$_x$(NO)$^+$ (X = 1−3), were probed by CID and SORI−CID. For example, the energy-resolved CID plot of CoH(CO)$_3$(NO)$^+$ is shown in Figure 4. In the low energy range, CID results in sequential elimination of the carbonyls. At high collision energy, formation of CoHNO$^+$ (three CO losses) dominates over Co(CO)$^+$ (two CO and one HNO losses). Previous studies on some mixed carbonyl−nitrosyl complexes have shown that the NO ligand is bonded more strongly to the metal center than the CO ligand. UV photolysis of Co(CO)$_3$(NO) yields CO loss to generate the primary photoproduct, Co(CO)$_2$(NO), which subsequently undergoes another CO loss to yield Co(CO)(NO).[31] These results are consistent with the observed CID fragmentation patterns. CID of CoH(CO)$_2$(NO)$^+$ is qualitatively similar to that for CoH(CO)$_3$(NO)$^+$.

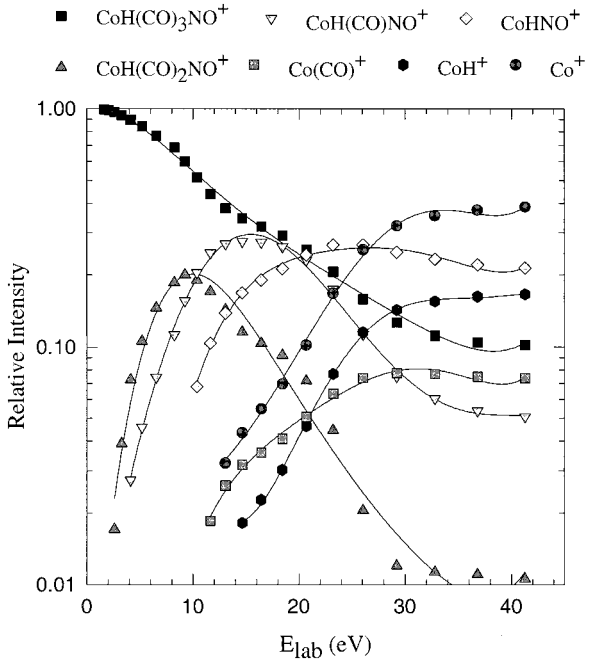

Figure 4. Energy-resolved CID breakdown curve of CoH(CO)$_3$NO$^+$.

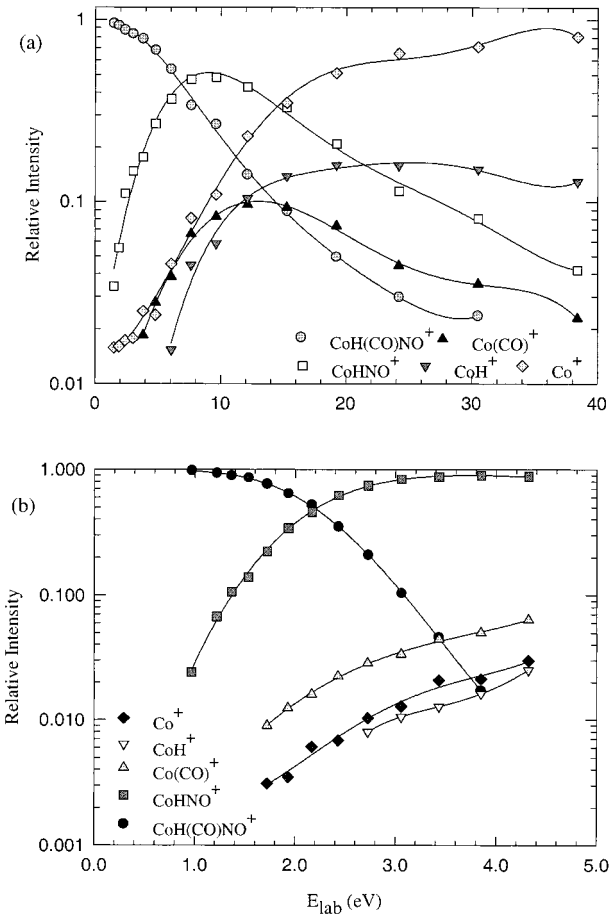

Figure 5. Energy-resolved CID (a) and SORI−CID (b) breakdown curves of CoH(CO)NO$^+$.

Competition between CO and HNO losses is observed during CID of CoH(CO)(NO)$^+$. The energy-resolved CID and SORI−CID plots of CoH(CO)(NO)$^+$ are shown in Figure 5. SORI−CID results clearly indicate that loss of CO to yield CoHNO$^+$ is the lowest energy decomposition channel, again, consistent with the weaker Co$^+$−CO bond. The complete absence of NO

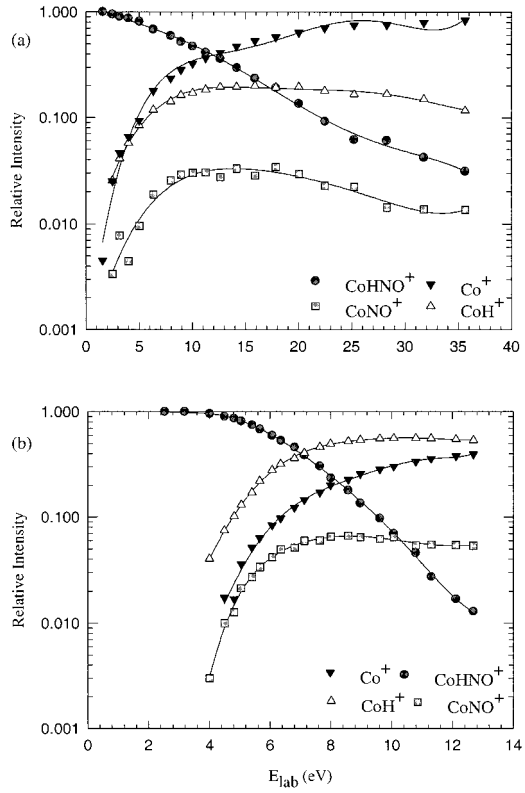

Figure 6. Energy-resolved CID (a) and SORI−CID (b) breakdown curves of $CoHNO^+$.

loss, combined with formation of $Co(CO)^+$ via HNO loss suggests that HNO is an intact ligand rather than separate H and NO bound to the metal; consequently, the structure is $Co(CO)(HNO)^+$. Competitive CO/HNO losses in SORI−CID suggest that $D°(Co^+-HNO)$ is ca. 1−2 kcal/mol greater than $D°(Co^+-CO) = 41.5 \pm 1.6$ kcal/mol.[32]

The structure of $CoHNO^+$ was further investigated by CID and SORI−CID, with reactions 9−11 observed.

$$CoHNO^+ \xrightarrow[SORI]{CID} Co^+ + HNO \quad (9)$$

$$\rightarrow CoNO^+ + H^{\cdot} \quad (10)$$

$$\rightarrow CoH^+ + NO \quad (11)$$

CID of $CoHNO^+$ (Figure 6) yields predominant Co^+ (HNO loss) over the entire kinetic energy range studied (0−35 eV). Formation of CoH^+ and $CoNO^+$ are competitive fragmentation channels. In contrast to CID, SORI−CID (Figure 6) yields CoH^+ (NO loss) in significant amount suggesting that NO loss is the lowest energy-demanding fragmentation channel. Competitive H and HNO losses are also observed at low energy.

A potential energy surface diagram for the decomposition of $CoHNO^+$ is shown in Figure 7. DFT calculations predict that $Co(HNO)^+$ (**2**) is the most stable species on the triplet surface, with $HCo(NO)^+$ (**1**) 14 kcal/mol higher. Upon collisional activation, **2** could rearrange to **1** where competitive ligand losses yield CoH^+ and $CoNO^+$, respectively. Alternatively, **2** could decompose to yield Co^+ and HNO, which requires about 45 kcal/mol. Under SORI−CID conditions, competitive formation of Co^+, CoH^+, and $CoNO^+$ suggests an activation barrier of about 40 kcal/mol for **2** → **1** conversion smaller than or very close to the 45 kcal/mol energy asymptote for HNO loss. As a result, rearrangement of **2** could be kinetically constrained under CID conditions and CID of **2** would then give predominant Co^+.

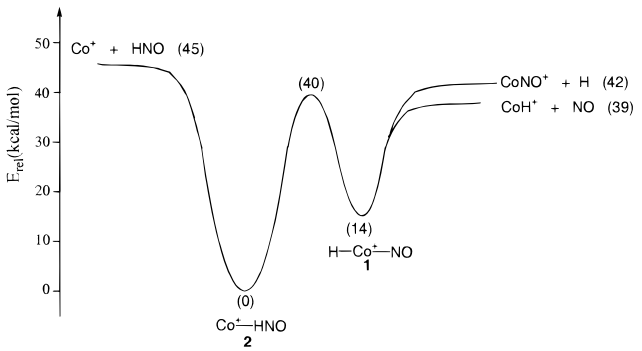

Figure 7. Potential energy surface diagram for the decomposition of $Co(HNO)^+$.

TABLE 2: Percentage Abundance of Primary Products, Rate Constants (cm^3 $molecule^{-1}$ s^{-1}), and Calculated Reaction Efficiencies for the Reactions of $Co(HNO)^+$ and $Co(DNO)^+$ with Selected Neutrals

ion	neutral	displacement	%	k_{obs}	k_{coll}	efficiency %
$CoHNO^+$	C_2H_2	NO	100	4.5×10^{-10}	9.5×10^{-10}	47
	C_2D_2	NO	100	4.3×10^{-10}	9.2×10^{-10}	47
	H_2O	NO	100	5.8×10^{-10}	1.9×10^{-9}	31
	C_4H_6	NO	100	4.9×10^{-10}	1.3×10^{-9}	38
	NH_3	NO	70	6.8×10^{-10}	1.8×10^{-9}	38
		HNO	30			
	NO	HNO	100	4.4×10^{-10}	8.8×10^{-10}	50
	CO	HNO	100	8.2×10^{-13}	7.3×10^{-10}	0.11
	CH_3CN	NO	80	1.9×10^{-9}	2.7×10^{-9}	70
		HNO	20			
	C_6H_6	HNO	100	1.6×10^{-9}	1.2×10^{-9}	130
$CoDNO^+$	C_2H_2	NO	100	4.1×10^{-10}	9.5×10^{-10}	43
	C_2D_2	NO	100	4.2×10^{-10}	9.2×10^{-10}	46

TABLE 3: Percentage Abundance of Primary Products, Rate Constants (cm^3 $molecule^{-1}$ s^{-1}), and Calculated Reaction Efficiencies for the Reactions of $Co(HNO)^+$ and $Co(DNO)^+$ with CH_4 and CD_4

ion	neutral	product	%	k_{obs}	k_{coll}	efficiency
$CoHNO^+$	CH_4	$CoCH_3NO^+$	100	7.5×10^{-12}	1.0×10^{-9}	0.75%
	CD_4	$CoDNO^+$	82	1.5×10^{-11}	1.0×10^{-9}	1.5%
		$CoCD_3NO^+$	18			
$CoDNO^+$	CH_4	$CoHNO^+$	83	2.9×10^{-11}	1.0×10^{-9}	2.9%
		$CoCH_3NO^+$	17			
	CD_4	$CoCD_3NO^+$	100	-	1.0×10^{-9}	-

2. Reactivity of CoHNO$^+$. The gas-phase reactivity of $CoHNO^+$ was explored by observing reactions of this ion with different neutral reagents. Product distributions and kinetic data for reaction with small molecules such as ethyne, benzene, methane, etc. are summarized in Tables 2 and 3.

Nitric Oxide and Carbon Monoxide. Nitric oxide (NO) reacts efficiently (50% of the collision rate) with $CoHNO^+$ by HNO displacement. Isotopically labeled NO (^{15}NO) reacts with $CoHNO^+$ in a similar fashion to yield $Co^{15}NO^+$ exclusively, reaction 12. No simple nitric oxide displacement (i.e., exchange) is observed, reaction 13. These results strongly support structure **2** or **3** for $CoHNO^+$, with **2**, $Co(HNO)^+$, most likely due to energetics. If $CoHNO^+$ consists of structure **1**, then we would expect to observe significant NO displacement, reaction 13, which is not observed.

$$CoHNO^+ + {}^{15}NO \rightarrow Co^{15}NO^+ + HNO \quad (12)$$

$$\not\rightarrow CoH^{15}NO^+ + NO \quad (13)$$

The potential energy surface diagram for reactions 12 and 13 is shown in Figure 8. While $D°(CoHNO^+-NO)$ is not

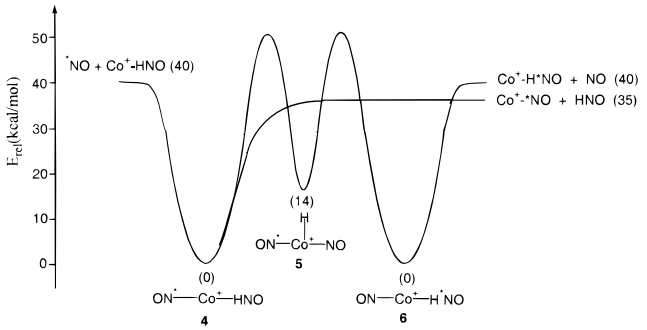

Figure 8. Potential energy surface diagram for the reaction of Co(HNO)$^+$ with ^{15}NO.

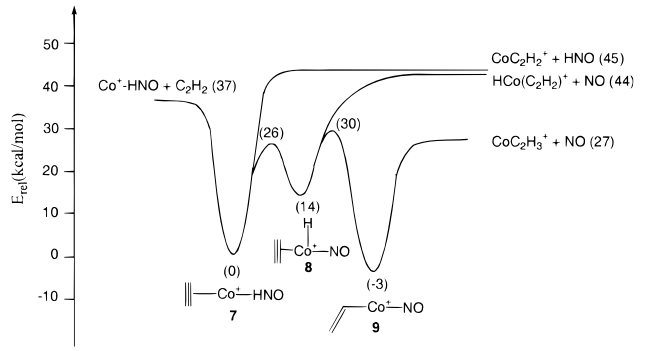

Figure 9. Potential energy surface diagram for the reaction of Co(HNO)$^+$ with C_2H_2.

known, $D°(Co^+-NO) = 40.0$ kcal/mol[27] provides a reasonable estimation. ^{15}NO coordination results in formation of **4** with roughly 40 kcal/mol excess energy. HNO elimination from **4** yields Co(^{15}NO)$^+$, reaction 12. Reaction 13 involves α-hydride migration in structure **2** to Co$^+$ to yield **5** with ∼26 kcal/mol excess energy. The reverse process involving hydride migration to ^{15}NO leads to the formation of **6** at the same energy level as **4**. NO elimination from **6** would yield Co(H^{15}NO)$^+$. Since reaction 13 is thermoneutral, then there must be a prohibitive barrier (>40 kcal/mol) for α-hydride migration to convert **4** to **5**.

Carbon monoxide reacts slowly (efficiency = 0.11%) with Co(HNO)$^+$ to yield HNO displacement (Table 2). This slow, direct HNO displacement suggests that it may be slightly endothermic. This result is consistent with SORI−CID of Co(CO)HNO$^+$ where both HNO and CO losses were observed, with CO loss dominating, Figure 5. Similar to the reaction with nitric oxide, there may be a substantial barrier for hydride migration from HNO to the metal center and from the metal center to CO.

Ethyne, 1,3-Butadiene, and Benzene. Reactions with ethyne, 1,3-butadiene, and benzene are discussed together even though there is no fixed reaction pattern among them. Ethyne and 1,3-butadiene yield NO displacement exclusively, while benzene yields HNO displacement exclusively, Table 2.

A potential energy surface diagram for (CoHNO)$^+$ with ethyne is presented in Figure 9. Coordination of ethyne to Co(HNO)$^+$ forms the collision complex, **7**, which has roughly 37 kcal/mol excess internal energy using $D°(Co^+-C_2H_2) = 37$ kcal/mol.[33] Direct cleavage of the Co$^+$−HNO bond requires ∼45 kcal/mol; consequently, it is roughly 8 kcal/mol endothermic. However, **7** can undergo hydride migration to form **8**, a nitrosyl complex ∼14 kcal/mol higher in energy than **7**. Direct NO elimination from **8** to yield HCo(CHCH)$^+$ is unlikely since it should be ∼7 kcal/mol endothermic. However, **8** can rearrange to **9**, a vinyl−nitrosyl complex. DFT calculations predict that

SCHEME 1

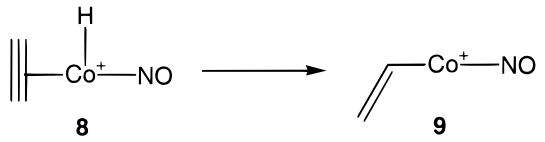

SCHEME 2

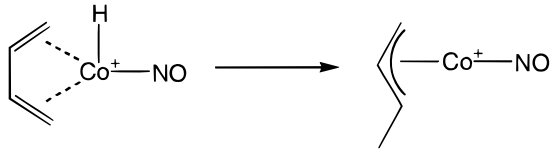

SCHEME 3

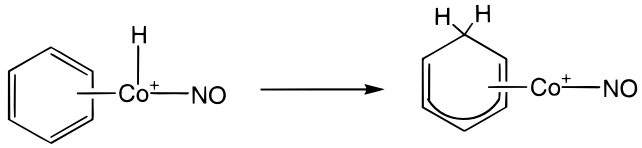

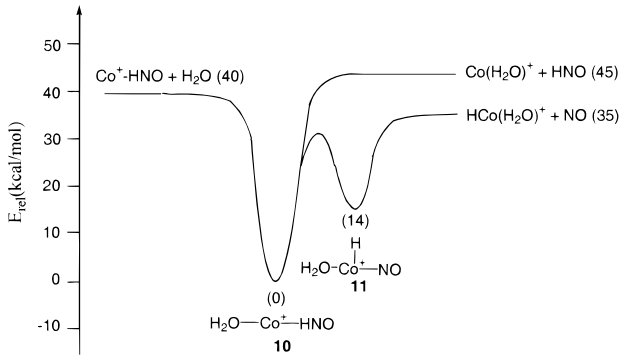

Figure 10. Potential energy surface diagram for the reaction of Co(HNO)$^+$ with H_2O.

Co(CHCH$_2$)$^+$ is ∼17 kcal/mol more stable than HCo(CHCH)$^+$. The activation barrier for HCo(CHCH)$^+$ → Co(CHCH$_2$)$^+$ conversion, although not obtained, is estimated to be less than 20 kcal/mol (ca. 16 kcal/mol).[34] Hence, **9** has 40 kcal/mol excess internal energy and can eliminate NO to yield Co(CHCH$_2$)$^+$. The energy for NO elimination from **9** must be less than the barrier for hydrogen migrations (**7** → **8** → **9**) since no H/D exchange was observed. This requires that $D°(CoC_2H_3^+-NO)$ be <30 kcal/mol.

The process analogous to **8** to **9** conversion (Scheme 1) could also occur for 1,3-butadiene (Scheme 2) and benzene (Scheme 3). The potential energy surface diagram for Co(HNO)$^+$ with 1,3-butadiene should be qualitatively similar to that for Co(HNO)$^+$ with ethyne where only NO displacement is observed. In the case of benzene, HNO and NO displacements are both exothermic because $D°(Co^+-C_6H_6) = 61.1 \pm 2.5$ kcal/mol.[35] That benzene yields only HNO displacement indicates that HNO elimination is kinetically favored even though intramolecular hydride migration to eliminate NO is energetically feasible. Hence, there must be a prohibitive barrier to hydride migration for the benzene collision complex.

Water, Ammonia, and Acetonitrile. Reactions with ammonia and acetonitrile yield both HNO and NO displacements with NO displacement dominating (Table 2). Reaction with water, however, yields NO displacement exclusively.

A potential energy surface diagram for the reaction of Co(HNO)$^+$ with H_2O is presented in Figure 10. Coordination of water to Co(HNO)$^+$ forms the collision complex, **10**, with 40

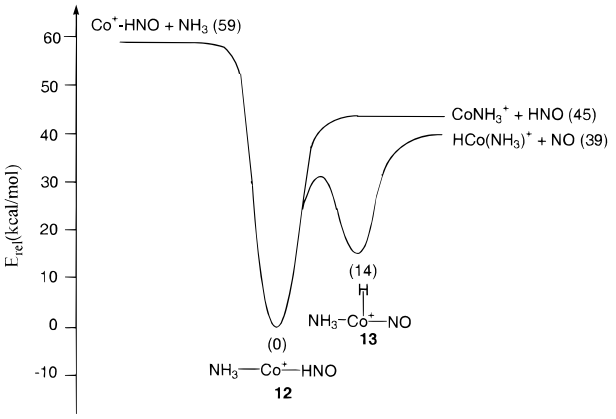

Figure 11. Potential energy surface diagram for the reaction of Co(HNO)$^+$ with NH_3.

kcal/mol excess internal energy using $D°(Co^+-H_2O) = 40.1$ kcal/mol.[36] HNO displacement is simply endothermic by ~5 kcal/mol. However, **10** to **11** conversion involves α-hydride migration from the HNO ligand to the metal center with a low activation barrier. NO elimination from **11** yields $HCo(H_2O)^+$ and is estimated to be exothermic by ~5 kcal/mol.

A potential energy surface diagram for the reaction of Co(HNO)$^+$ with ammonia is presented in Figure 11. The collision complex, **12**, is formed with 59 kcal/mol excess internal energy using $D°(Co^+-NH_3) = 58.8$ kcal/mol.[36] Direct HNO elimination (30%) from **12** is exothermic by ~14 kcal/mol. Structure **12** could rearrange to **13** with 45 kcal/mol excess internal energy. NO elimination (70%) from **13** to yield $HCo(NH_3)^+$ is estimated to be exothermic by 20 kcal/mol, 6 kcal/mol more exothermic than the HNO displacement channel.

Reaction with acetonitrile yields 80% NO displacement and 20% HNO displacement. The potential energy surface for this reaction should be qualitatively similar to that for ammonia.

Methane. Co(HNO)$^+$ reacts with methane to form $CoCH_3NO^+$ (H_2 loss), reaction 14.

$$CoHNO^+ + CH_4 \rightarrow CoCH_3NO^+ + H_2 \qquad (14)$$

Methane activation is rare for the first-row transition metal complexes. Some second-row and third-row transition-metal ions or ion complexes, such as Ta^+ and $RhCH_2^+$, react with methane by dehydrogenation.[37] Many cobalt ion complexes, for example, $CoCH_2^+$, $CoCH_3^+$, $CoCF_3^+$ etc., are inert toward methane.[38] Therefore, activation of methane by Co(HNO)$^+$ is surprising. Pseudo-first-order kinetics is observed for reaction 14, and a kinetic plot for the reaction of Co(HNO)$^+$ with CH_4 is shown in Figure 12. The primary product distributions and kinetic information for the reactions of Co(HNO)$^+$/Co(DNO)$^+$ with CH_4/CD_4 are summarized in Table 3. In addition to dehydrogenation, H/D exchange was also observed. For example, $CoHNO^+$ reacts with CD_4 to yield $CoDNO^+$ predominantly along with some $CoCD_3NO^+$, reactions 15 and 16.

$$CoHNO^+ + CD_4 \rightarrow CoDNO^+ + CD_3H \qquad (15)$$

$$\rightarrow CoCD_3NO^+ + HD \qquad (16)$$

$CoCH_3NO^+$, generated in reaction 14, was subjected to CID and SORI−CID for structural investigation. CID of $CoCH_3NO^+$ (Figure 13) yields $CoCH_3^+$ (NO loss), $CoNO^+$ (CH_3 loss), and Co^+ (CH_3NO loss). SORI−CID of $CoCH_3NO^+$ (Figure 13) yields $CoCH_3^+$ exclusively, consistent with $D°(Co^+-CH_3) = 53.3 \pm 2$ kcal/mol[39] > $D°(Co^+-NO) = 40.0$ kcal/mol.[27] These results suggest that $CoCH_3NO^+$ has the structure CH_3CoNO^+, containing two intact ligands, CH_3 and NO. Although Co(HNO)$^+$, **2**, is predicted to be 14 kcal/mol more stable than HCo(NO)$^+$, **1**, CH_3CoNO^+ apparently is thermodynamically more stable than the corresponding $Co(CH_3NO)^+$ structure. A comparison of relevant fundamental bond dissociation energies supports this idea.[40] In any case, the ion formed in reaction 14 has the structure, CH_3CoNO^+.

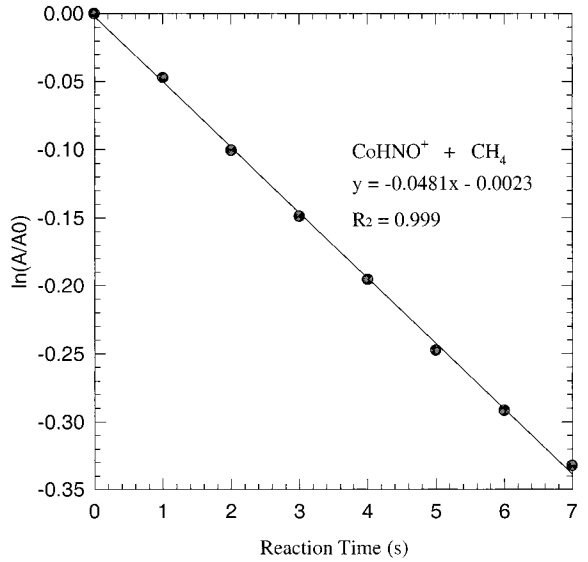

Figure 12. Pseudo-first-order plot of the reaction of Co(HNO)$^+$ with methane at 2.0×10^{-7} Torr.

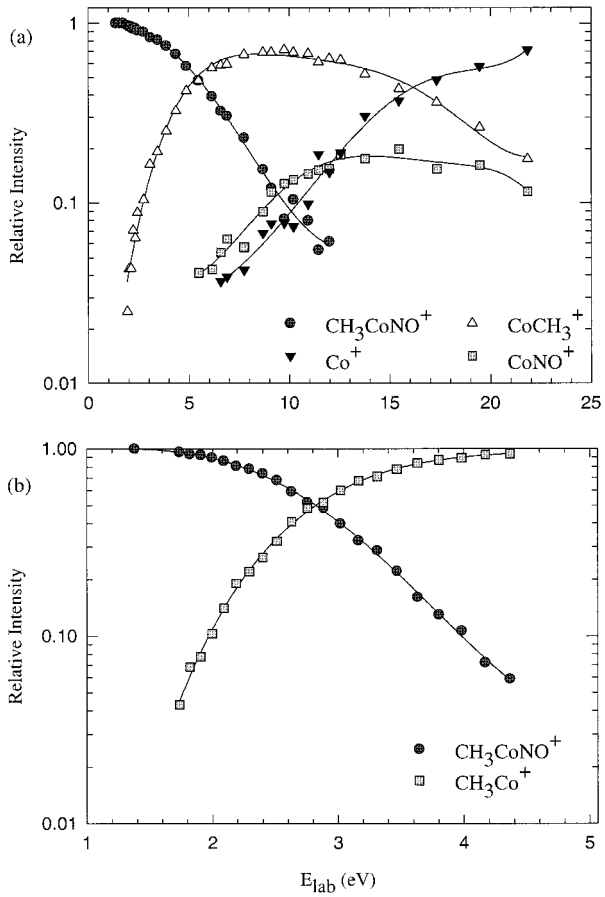

Figure 13. Energy-resolved CID (a) and SORI−CID (b) breakdown curves of CH_3CoNO^+.

SCHEME 4

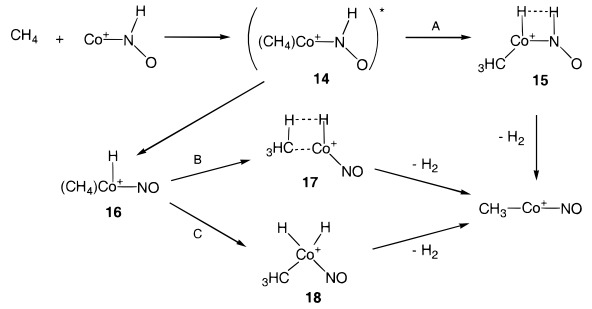

SCHEME 5

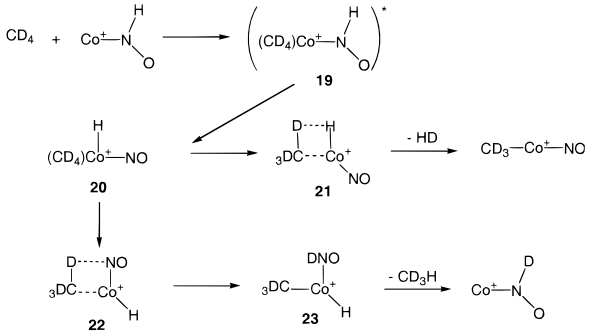

We now consider the mechanism for reaction 14, as well as that for reactions 15 and 16. A proposed mechanism for reaction 14 is shown in Scheme 4. Several routes can lead to the formation of CH_3CoNO^+. In route A, the collision complex, **14**, may undergo dehydrogenation through the four-centered transition state, **15**, to yield CH_3CoNO^+. Routes B and C share the same intermediate, **16**, formed by an initial α-hydride migration from the HNO ligand to the metal center. In route B, dehydrogenation proceeds through the four-centered transition state, **17**, to yield CH_3CoNO^+. Route C, however, involves direct C−H insertion yielding **18** followed by dehydrogenation to yield CH_3CoNO^+.

Using $D°(Co^+-CH_4) = 22.9 \pm 0.7$ kcal/mol,[41] the collision complex, **14**, is formed with roughly 20 kcal/mol excess internal energy. Both Co^+ and CoH^+ are inert with methane even though reaction 17 is exothermic by $\sim 12 \pm 4$ kcal/mol.[40]

$$CoH^+ + CH_4 \rightarrow CoCH_3^+ + H_2 \qquad (17)$$

These results suggest a prohibitive barrier associated with direct C−H insertion for **14** → **15** or **16** → **18** conversion. However, activation of methane through the four-centered transition state, **17**, precludes direct C−H bond insertion. This type of four-centered transition state has been proposed in previous studies. Watson observed an interesting methane exchange reaction proceeding through a four-centered transition state.[42] In addition, Jacobson has studied the dehydrogenation reaction of $RhCH_2^+$ with methane proceeding through a four-centered transition state.[37b] Therefore, we think the mechanism associated with route B is more likely.

A proposed mechanism for reactions 15 and 16 is presented in Scheme 5 and is based on pathway B in Scheme 4. The collision complex **19** first converts to **20** by α-hydride migration. HD loss may proceed by the four-centered transition state, **21**. H/D exchange may involve the four-centered transition state, **22**, which yields **23** followed by methane reductive elimination. H/D exchange through **22** dominates over HD loss through **21**.

Summary

$CoHNO^+$ is generated in the gas phase by CID or SORI−CID of $CoH(CO)_3NO^+$, formed from chemical ionization of $Co(CO)_3NO$ with CH_5^+. Among the three isomeric structures, $HCo(NO)^+$ (**1**), $Co(HNO)^+$ (**2**), and $Co(NOH)^+$ (**3**), density functional calculations found that **2** is the global minimum on the potential energy surface with **1** and **3** 14.1 and 15.4 kcal/mol higher in energy. Reaction of $CoHNO^+$ with isotopically labeled NO (^{15}NO) yields HNO displacement exclusively, which strongly supports a structure with an intact HNO ligand, either **2** or **3**. Owing to energetics, the structure is most likely **2**. CID of $Co(HNO)^+$ yields Co^+ predominantly along with $CoNO^+$ and CoH^+. In contrast, SORI−CID of $Co(HNO)^+$ yields significant CoH^+. Although the transition state for the **2** → **1** conversion is not located, CID and SORI−CID of $CoHNO^+$ suggest that the activation barrier for **2** → **1** conversion is less than 45.5 kcal/mol.

The reactivity of $Co(HNO)^+$ was explored by observing its reactions with simple molecules. These reactions are dominated by NO and HNO displacements. For example, $Co(HNO)^+$ reacts with ethyne, water, and 1,3-butadiene to yield NO displacement exclusively. Reaction with nitric oxide, carbon monoxide, and benzene yields HNO displacement exclusively. Reaction with ammonia and acetonitrile yields both HNO and NO displacements with NO displacement dominating. Potential energy surface diagrams for these NO and HNO displacement reactions are presented which consistently involve α-H migration from the HNO ligand to the metal center. $Co(HNO)^+$ reacts with methane by dehydrogenation to yield $CoCH_3NO^+$. While CID of $CoCH_3NO^+$ yields competitive formation of $CoCH_3^+$ and $CoNO^+$, SORI−CID of $CoCH_3NO^+$ yields $CoCH_3^+$ exclusively. These results suggest $CoCH_3NO^+$ has structure CH_3CoNO^+ rather than $Co(CH_3NO)^+$. A mechanism is proposed for the reaction with methane where a four-centered transition state is involved for C−H bond activation as opposed to direct C−H insertion.

Acknowledgment. This paper is dedicated to the memory of Dr. Ben S. Freiser. Acknowledgment is made to the Division of Chemical Sciences in the Office of Basic Energy Sciences in the United States Department of Energy (Grant No. DE-FG02-87ER13766) for supporting this research.

References and Notes

(1) (a) Collman, J. P.; Hegedus, L. S.; Norton, J. R.; Finke, R. G. *Principles and Applications of Organotransition Metal Chemistry*; University Science Book: Mill Valley, CA, 1987. (b) Cotton, F. A.; Wilkinson, G. In *Advanced Inorganic Chemistry*; Wiley: New York, 1988.

(2) Roe, D. C. *J. Am. Chem. Soc.* **1983**, *105*, 7770.

(3) Sakaki, S.; Kato, H.; Kanai, H.; Tarama, K. *Bull. Chem. Soc. Jpn.* **1975**, *48*, 813.

(4) Dombek, B. D. *J. Am. Chem. Soc.* **1980**, *102*, 6855.

(5) Nakamura, S.; Morokuma, K. *Abstracts*, 33rd Symposium on Organometallic Chemistry, Japan: Tokyo, Japan, October 1986; paper A109.

(6) (a) Herrmann, W. A. *Angew. Chem., Int. Ed. Engl.* **1982**, *21*, 117. (b) Blackborow, J. R.; Daroda, R. J.; Wilkinson, G. *Coord. Chem. Rev.* **1982**, *43*, 17.

(7) (a) Grimmett, D. L.; Labinger, J. A.; Bonfiglio, J. N.; Masuo, S. T.; Shearin, E.; Miller, J. S. *Organometallics* **1983**, *2*, 1325. (b) Masters, C. *Adv. Organomet. Chem.* **1979**, *17*, 61. (c) Fahey, D. R. *J. Am. Chem. Soc.* **1981**, *103*, 136.

(8) (a) Wayland, B. B.; Woods, B. A. *J. Chem. Soc., Chem. Commun.* **1981**, 700. (b) Farnos, M. D.; Woods, B. A.; Wayland, B. B. *J. Am. Chem. Soc.* **1986**, *108*, 3659.

(9) Canestrari, M.; Green, M. L. H. *J. Chem. Soc., Dalton Trans.* **1982**, 1789.

(10) Ziegler, T.; Versluis, L.; Tschinke, V. *J. Am. Chem. Soc.* **1986**, *108*, 612.

(11) Carter, E. A.; Goddard, W. A. *J. Am. Chem. Soc.* **1987**, *109*, 579.

(12) Richter-Addo, G. B.; Legzdins, P. In *Metal Nitrosyls*; Oxford University Press: New York, 1992.
(13) Wilson, R. D.; Ibers, J. A. *Inorg. Chem.* **1979**, *18*, 336.
(14) Stevens, R. E.; Guettler, R. D.; Gladfelter, W. L. *Inorg. Chem.* **1990**, *29*, 451.
(15) Gord, J. R.; Freiser, B. S. *Anal. Chim. Acta* **1989**, *225*, 11.
(16) Freiser, B. S. *Talanta* **1985**, *32*, 697.
(17) Gauthier, J. W.; Trautman, T. R.; Jacobson, D. B. *Anal. Chim. Acta* **1991**, *246*, 211.
(18) Grosshans, P. B.; Marshall, A. G. *Anal. Chem.* **1991**, *63*, 2057.
(19) Freiser, B. S. *Techniques for the Study of Ion Molecule Reactions*; Farrar, J. M., Saunders, W. H., Jr., Eds.; Willey: New York, 1988; p 61.
(20) Frisch, M. J.; Trucks, G. W.; Schlegel, H. B.; Gill, P. M. W.; Johnson, B. G.; Robb, M. A.; Cheeseman, J. R.; Keith, T.; Petersson, G. A.; Montgomery, J. A.; Raghavachari, K.; Al-Laham, M. A.; Zakrzewski, V. G.; Ortiz, J. V.; Foresman, J. B.; Peng, C. Y.; Ayala, P. Y.; Chen, W.; Wong, M. W.; Andres, J. L.; Replogle, E. S.; Gomperts, R.; Martin, R. L.; Fox, D. J.; Binkley, J. S.; Defrees, D. J.; Baker, J.; Stewart, J. P.; Head-Gordon, M.; Gonzalez, C.; Pople, J. A. *Gaussian 94*, Revision D.1 Gaussian, Inc.: Pittsburgh, PA, 1995.
(21) (a) Becke, A. D. *Phys. Rev.* **1988**, *A38*, 3098. (b) Becke, A. D. *J. Chem. Phys.* **1993**, *98*, 1372. (c) Becke, A. D. *J. Chem. Phys.* **1993**, *98*, 5648.
(22) Wachters, A. J. H. *J. Chem. Phys*. **1970**, *52*, 1033.
(23) Bauschlicher, C. W.; Langhoff, S. R., Jr.; Barnes, L. A. *J. Chem. Phys.* **1989**, *91*, 2399.
(24) Dunning, T. H., Jr. *J. Chem. Phys.* **1989**, *90*, 1007.
(25) Ziegler, T.; Li, J. *Can J. Chem.* **1994**, *72*, 783.
(26) (a) Bauschlicher, C. W., Jr.; Patridge, H. *Chem. Phys. Lett.* **1995**, *240*, 533. (b) Ricca, A.; Bauschlicher, C. W., Jr. *Chem. Phys. Lett.* **1995**, *245*, 150. (c) Heinemann, C.; Hertwig, R. H.; Wesendrup, R.; Koch, W.; Schwarz, H. *J. Am. Chem. Soc.* **1995**, *117*, 495. (d) Holthausen, M. C.; Fiedler, A.; Schwarz, H.; Koch, W. *J. Phys. Chem.* **1996**, *100*, 6236.
(27) Thomas, J. L. C.; Bauschlicher, C. W.; Hall, M. B. *J. Phys. Chem. A* **1997**, *101*, 8530.
(28) Clement, M. J. Y.; Ramsay, D. A. *Can. J. Phys.* **1961**, *39*, 205.
(29) Huber, K. P.; Herzberg, G. *Molecular Spectra and Molecular Structure Constants of Diatomic Molecules*; Van Nostrand: New York, 1979.
(30) Smolyar, A. E.; Zaretskii, N. P.; Charkin, O. P. Zh. *Neorg. Khim.* **1979**, *24*, 3160.
(31) Gadd, G. E.; Poliakoff, M.; Turner, J. J. *Organometallics* **1987**, *6*, 391.
(32) Goebel, S.; Haynes, C. L.; Khan, F. A.; Armentrout, P. B. *J. Am. Chem. Soc.* **1995**, *117*, 6994.
(33) Sodupe, M.; Bauschlicher, C. W. *J. Chem. Phys.* **1991**, *95*, 8640.
(34) Chen, H.; Jacobson, D. B.; Freiser, B. S., paper in preparation.
(35) Meyer, F.; Khan, F. A.; Armentrout, P. B. *J. Am. Chem. Soc*. **1995**, *117*, 9740.
(36) Squires, R. R. *J. Am. Chem. Soc*. **1989**, *111*, 4101.
(37) (a) Buckner, S. W.; MacMahon, T. J.; Byrd, G. D.; Freiser, B. S. *Inorg. Chem.* **1989**, *28*, 3511. (b) Jacobson, D. B.; Freiser, B. S. *J. Am. Chem. Soc.* **1985**, *107*, 5870.
(38) (a) Jacobson, D. B.; Freiser, B. S. *J. Am. Chem. Soc.* **1985**, *107*, 4373. (b) Jacobson, D. B.; Freiser, B. S. *J. Am. Chem. Soc.* **1984**, *106*, 3891. (c) Chen, Q.; Lin, C.-Y.; Chen, H.; Freiser, B. S. *Organometallics* **1997**, *16*, 4020.
(39) van Koppen, P. A. M.; Kemper, P. R.; Bowers, M. T. *J. Am. Chem. Soc.* **1993**, *115*, 5616.
(40) Calculations are based on thermochemical data taken from the reference: Lias, S. G.; Bartmess, J. E.; Liebman, J. F.; Holmes, J. L.; Levin, R. D.; Mallard, W. G. Gas-Phase Ion and Neutral Thermochemistry *J. Phys. Chem. Ref. Data*. **1988**, 17, Suppl. No. 1.
(41) Kemper, P. R.; Bushnell, J. E.; van Koppen, P. A. M.; Bowers, M. T. *J. Phys. Chem.* **1993**, *97*, 1810.
(42) Watson, P. L. *J. Am. Chem. Soc*. **1983**, *105*, 6491.